Parametric Study for Conductor Design of KSTAR PF Coils

Cheon Seog Yoon*
Department of Mechanical Engineering, Hannam University, Taejon 306-791, Korea
Qiuliang Wang, Myungkyu Kim, Keeman Kim**
Energy Lab. , Samsung Advanced Institute of Technology, Taejon 305-380, Korea
**(Present Address : Institute of Electrical Engineering, Chinese Academy of Sciences, Beijing, 100080, P. R. China)*
Dong-Ryul Lee
School of Automotive and Mechanical Engineering, Catholic University of Taegu, Kyungsan, Taegu 712-702, Korea

Large superconducting magnets such as ITER (International Thermonuclear Experimental Research) or KSTAR (Korean Superconducting Tokamak Advanced Research) magnet system adopted a cable-in-conduit conductor (CICC) using a forced-flow cooling system. Main optimization criteria for the conductor design of superconducting magnet system are stability margin and CICC cooling requirements. A zero-dimensional method is applied for the calculation of stability and the conductor optimization. In order to increase conductor performance, three different strands, ITER HP-I and HP-II, and KSTAR HP-III, are tested. The strand characteristics of KSTAR HP-III are measured in the Samsung's PPMS and Jc measurement system, and applied for this study. Also, the strand diameters, 0.81 mm and 0.78 mm are considered for this study, due to design change. Based on this result, the proposed configuration of CICC has been fabricated.

Key Words : Superconducting Magnet, CICC, Stability, Conductor Performance

1. Introduction

The KSTAR device has 14 PF (Poloidal Field) coils of circular shape and 16 TF (Toroidal Field) coils of D-shape. General arrangement of KSTAR magnet with vacuum vessel is shown in Fig. 1.

The coil system consists of many winding packs of cable-in-conduit conductor. Large superconducting magnets can be cooled either by immersing them in a pool of boiling helium or by circulating helium through passages in the conductor. Cable-in-conduit conductors (CICC) using forced-flow cooling system have been widely used for superconducting magnet with cryogenic cooling environment; these CICC's consist of superconducting strands surrounded by supercritical helium. The helium is used to cool the superconductor during steady-state operation.

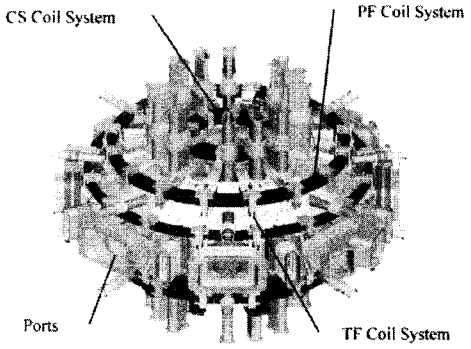

Fig. 1 KSTAR magnet system with vacuum vessel

* Corresponding Author,
E-mail : csyoon@mail.hannam.ac.kr
TEL : +82-42-629-8283; **FAX** : +82-42-629-8043
Department of Mechanical Engineering, Hannam University, Taejon 306-791 Korea. (Manuscript **Received** March 20, 2001; **Revised** October 30, 2001)

Superconducting strands and helium are surrounded by a conduit, which is generally made of stainless steel or Incoloy 908.

The conductor is stable if the conductor recovers its superconducting state after a disturbance. If the disturbance exceeds certain limits, it does not recover from normal to superconducting state, and quench occurs. After a quench is detected, the stored magnetic energy is normally released in a dump circuit to protect the magnet system. Numerous researches (Seeber, 1998) have been done for accurate stability analysis and quench characteristics in forced flow cooling type CICC. Because there are coupled compressible helium flow and heat diffusion in complex geometry, the calculation of stability margin is a difficult task. Thus, simplified models have been developed for practical purpose. These are classified one-dimensional, zero-dimensional, and energy balance models. Though one-dimensional model (Marinucci, 1983, Bottura, 1995, Wang, 2000) can handle complex geometry in CICC, the disadvantage is slow convergence and difficulty to handle, due to large different time scales. Zero-dimensional model use the simplification of one-dimensional model, which neglect the length effect and assume that energy balance between heat production and accumulation holds locally. The main advantage of this model is simplicity, efficiency, and routine nature. Energy balance model (Dresner, 1981) can be obtained by replacing time-dependent power balances of the zero-dimensional model with time-independent energy and power balance in the cross-section. This method supplies a rough estimation of the stability margin and produces easy-to-apply design criteria for the selection of the cable layout. But it is too crude to use parametric study for practical purpose.

Superconducting coils experience instability caused by the energy perturbations such as motions of conductors and strands, cracks of structure or insulation materials, and AC (alternating current) losses. Key issues of CICC design are stability margin and maximum pressure, hot-spot temperature, and mass flow rate under quench condition. This study utilizes a zero-dimensional model to execute stability analysis and parametric study for Nb3Sn cables, ITER HP-I and HP-II, and KSTAR HP-III. Measured data of KSTAR HP-III strands are obtained from Samsung, and applied for this study. Also, these simulations are considered for the various conditions of operating current, initial temperature, void fraction, operating field, and pulse duration.

2. Strand Characteristics

2.1 Critical temperature

The critical temperature of Nb_3Sn is a function of the applied magnetic field and it can be obtained by linear approximation of $T_c(B)$ relation (Anderson, 1983):

$$T_c = T_{c0}\left(1-\frac{B}{B_{c20}}\right) \tag{1}$$

where T_{c0} is the critical temperature at zero magnetic field and B_{c20} is the critical field at zero temperature. These two parameters are functions of the longitudinal strain applied to the superconducting filament ε through relations :

$$T_{c0} = T_{c0M}(1-a\,|\,\varepsilon\,|^{1.7})^{\frac{1}{3}} \tag{2}$$

$$B_{c20} = B_{c20M}(1-a\,|\,\varepsilon\,|^{1.7}) \tag{3}$$

where T_{c0M} and B_{c20M} are the values of T_{c0} and B_{c20} for a strain-free filament. These values are in Table 2, which represents the performance coefficients of Nb_3Sn for ITER HP-I and HP-II, and KSTAR HP-III, and the value of a is a function of ε and is given by:

$$a=\begin{pmatrix}1250 \text{ for } \varepsilon>0, \text{ tention}\\ 900 \text{ for } \varepsilon<0, \text{ compression}\end{pmatrix} \tag{4}$$

2.2 Critical current density

The critical current density of Nb_3Sn is described by following functions of temperature and field (Anderson, 1983):

$$J_c = C_0\frac{1}{\sqrt{bB_{c2}}}(1-b)^2(1-t^2)^2 \tag{5}$$

with:

$$t=\frac{T}{T_{c0}},\quad b=\frac{B}{B_{c2}} \tag{6}$$

where B_{c2} is given by:

Table 1 Measured data for KSTAR HP-III strands

Manufacturer/ Strands Test Condition	Critical Current Density Jc (A/mm^2) @12T, 0.1 (V/cm, 4.2 K	Hysteresis Loss Qh (mJ/cc) @±3T
IGC HP-III	874	252
MELCO HP-III (Type A)	995	164
MELCO HP-III (Type B)	1,024	216

Table 2 Performance coefficients for Nb_3Sn

Nb_3Sn	B_{c20M}	T_{c0M}	C_0
	(T)	(K)	(A-T/mm^2)
ITER HP-I	28	18	11,600
ITER HP-II	28	18	9,064
KSTAR HP-III	28	18	12,400

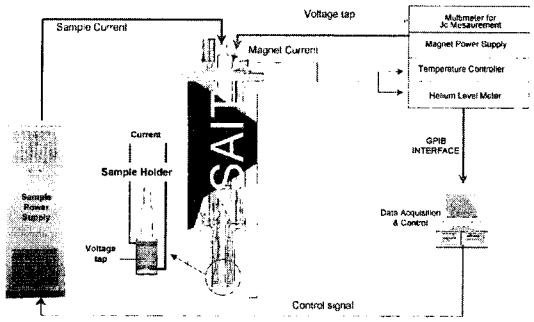

Fig. 2 Critical current measurement system in Samsung

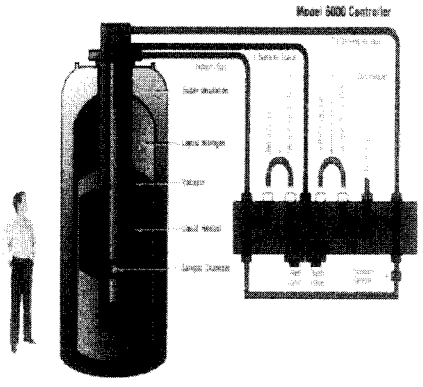

Fig. 3 Schematics of PPMS-9 in Samsung (Quantum Design, USA)

$$B_{c2}=B_{c20}(1-t^2)\left(1-\frac{1}{3}t\right) \quad (7)$$

The material and geometrical constant C_0 is a property of the particular form of Nb_3Sn and the ratio of the cross sectional areas of superconductor and non-copper. In order to get adequate performance coefficient of KSTAR HP-III strands, HP-III strands of IGC (Intermagnetics General Corporation) and MELCO (Mitsubishi Electric Corporation) were tested by Samsung's critical current measurement system in Fig. 2 and ACMS (AC Measurement System) option of PPMS (Physical Property Measurement System) in Fig. 3. Because of the uncertainty for the development stage of KSTAR HP-IIII, the minimum specification of KSTAR HP-III strand were required that critical current density should be greater than 750 A/mm^2 at 12 T, 4.2 K, 0.1 $\mu V/cm$, and AC loss should be less than 250 mJ/cc per ±3 T cycles. Figure 4 shows raw data of the critical current density and hysteresis loss for HP -III strands of IGC and MELCO. Here, type A and B of MELCO represents only the origin of strands from different rods. In Table 1, summarized data of KSTAR HP-III are sufficiently satisfied by the requirement of strand specification and applied for this study. From these experimental data and previous fitting vales, the performance coefficients of Nb_3Sn are in Table 2 (SAIT, 1999).

3. Numerical Model

The CICC for KSTAR PF Coils, fabricated by HP-III strands and jacketed by Incoloy 908, is in

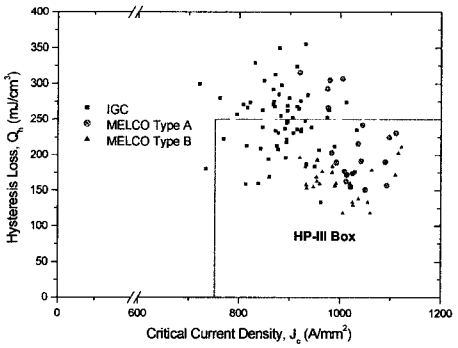

Fig. 4 Critical current density at 12 T vs. hysteresis loss measured at 4.2K, ±3T

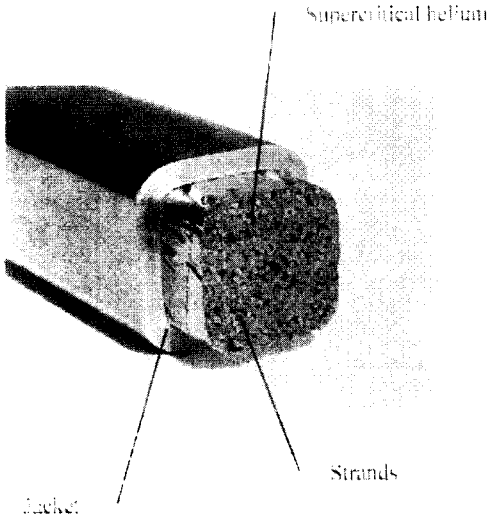

Fig. 5 CICC geometry, fabricated by KSTAR HP-III

Fig. 5. Detailed components of CICC are supercritical helium, strands, and jacket. CICC is approximated into single degree-of-freedom by each component, through the lumping model (Bottura, 1997). Based on a local heat balance, the governing equations for strands, jacket, and helium are as below:

$$A_{st}C_{st}\frac{dT_{st}}{dt}=\dot{q}'_{st}+\dot{q}'_{joule}-p_{st,he}h_{st,he}(T_{st}-T_{he})-p_{st,ja}h_{st,ja}(T_{st}-T_{ja}) \quad (8)$$

$$A_{ja}C_{ja}\frac{dT_{ja}}{dt}=-p_{ja,he}h_{ja,he}(T_{ja}-T_{he})-p_{st,ja}h_{st,ja}(T_{ja}-T_{st}) \quad (9)$$

$$A_{he}C_{he}\frac{dT_{he}}{dt}=\dot{q}'_{ja}+p_{st,he}h_{st,he}(T_{st}-T_{he})+p_{ja,he}h_{ja,he}(T_{ja}-T_{he}) \quad (10)$$

where subscripts *st*, *ja*, *he* represent strands, jacket, and helium, respectively. Three components, with cross-sectional area, A, have heat capacities, C, that are computed for each component of cable as the sum of copper and superconductor (strands), steel and insulation (jacket), and the full helium cross-sectional area. The components are thermally coupled through convection on wetted surfaces, p, with a surface heat transfer coefficients, h, which are defined as below (Bottura, 1991) ;

$$h_{st,he}=h_{he} \quad (11)$$

$$h_{ja,he}=\frac{h_{ja}h_{he}}{h_{ja}+h_{he}} \quad (12)$$

$$h_{st,ja}=\frac{h_{ja}h_{co}}{h_{ja}+h_{co}} \quad (13)$$

with the following definitions

$$h_{he}=\max\{h_{Ks},\ h_{Kt}\} \quad (14)$$

$$h_{Kt}=\frac{h_K h_t}{h_K+h_t} \quad (15)$$

$$h_{Ks}=\frac{h_K h_{ss}}{h_K+h_{ss}} \quad (16)$$

$$h_K=200(T_{st}+T_{he})(T_{st}^2+T_{he}^2) \quad (17)$$

$$h_t=\sqrt{\frac{K\rho C_p}{\pi t}} \quad (18)$$

K, ρ, C_p, h_{ss} are thermal conductivity, density, specific heat at constant volume, and steady state heat transfer coefficient of helium, respectively. Empirical definitions for thermal contacts of strands and jacket are

$$h_{ja}=\frac{2K_{ss}}{t_{ss}} \quad (19)$$

$$h_{co}=1000 \quad (20)$$

where K_{ss} is the thermal conductivity of the stainless steel or Incoloy908 and t_{ss} is the thickness of the jacket.

During the evolution, the initial energy input is the strands $\dot{q}'_{st}$ or in the jacket $\dot{q}'_{ja}$ causes the cable to transit to the normal state. The system of Eqs. (8) to (10) is solved by an implicit, linearized, first order accurate algorithm that is unconditionally stable. Adaptive time stepping is used.

4. Results and Discussions

Input parameters for this study are listed in Table 3, which represents conductor parameters and operating conditions of KSTAR PF coils. The strand diameter was 0.81 mm in the old design (KBSI, 1997), but it was reduced to 0.78 mm in the new design (SAIT, 1999), due to fabrication problem of strand drawing. The void fraction was changed from 34.4 % to 39.3 % and the area of superconductor and copper was reduced by 7.4 % from the old design. As the void fraction is increased, the AC coupling loss of the CICC is reduced and the helium area is increased;

Table 3 Conductor parameters & operating conditions

Parameter	Unit	Old Design (PF1-5)	New Design (PF1-5)
Conductor		Nb_3Sn (ITER HP-I)	Nb_3Sn (KSTAR HP-III)
Conduit		Incoloy908	Incoloy908
Cu/Non-Cu		1.5:1	1.5:1
Aconduit	mm^2	179.2	175.6
Dstrand	mm	0.81	0.78
nstrands		360	360
ncustrands		120	120
hconduit	mm	22.3	22.3
wconduit	mm	22.3	22.3
tconduit	mm	2.41	2.41
Acu	mm^2	136.04	126.1
Anoncu	mm^2	49.47	45.8
Ahecond	mm^2	97.28	111.4
$n\tau$(B=0)	ms	60	60
RRR		100	100
Pin	atm	5	5
Tin	K	5	5
Iop, max	kA	26.5	26.5
Bmax	T	7.8	7.8

thus, the stability margin is increased due to rapid heat transfer and available helium enthalpy. Here, the definition of the stability margin for a CICC is the largest sudden heat input that the conductor is able to absorb and still recover the superconducting state. Simplified formula of the stability margin is defined by the available helium enthalpy (Lue, 1994):

$$\Delta H=\frac{A_{he}}{A_{co}}\int_{T_b}^{T_{cs}} C_p dT \qquad (21)$$

where T_{cs}, T_b, A_{co}, C_p are current-sharing temperature of superconductor, ambient helium temperature, conductor cross-sectional area, and helium specific heat, respectively. ZERODEE (Bottura, 1997), commercially available software for stability analysis, is used to calculate the stability margin. It handles the variables of superconductor area, copper area, helium area, steady state heat transfer coefficient, strain, RRR of copper, field, operating current, pulse duration, initial pressure, and initial temperature. This study is focused on operating current, initial temperature, field, and pulse duration for different Nb_3Sn strands, ITER HP-I and HP-II, and KSTAR HP-III and design variations. Measured

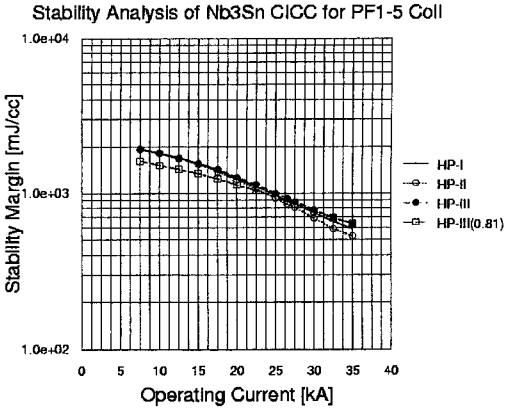

Fig. 6 Operating current vs. stability margin

data of KSTAR HP-III are obtained from the experiment of Samsung Advanced Institute of Technology and applied for this study.

Figure 6 shows the dependence of stability margin on operating current. The inlet pressure, inlet temperature, field, and pulse duration are 5 atm, 5 K, 7.8 T, and 60 ms, respectively. The geometric configurations are the same as in Table 3, except for the operating current. At 26.5 kA of the operating current, the stability margins of HP-III, HP-II, and HP-I for the new design are 928, 848, and 893 mJ/cc, respectively. Also, its value for the old design is 880 mJ/cc and the difference is about 50 mJ/cc. As expected, stability margin of HP-III for new design is greater than the design criteria of KSTAR magnet, because $E_{headroom}$ and E_{margin} are 600 and 300 mJ/cc. The definitions of $E_{headroom}$ and E_{margin} are in the Table 4 (PPPL, 1996). Since the critical current density is only considered to this calculation, except AC loss, the magnitude of the stability margin for Nb_3Sn strands is HP-III, HP-I, and HP-II, as a descending order and their trends of the curves are physically reasonable. As the operating current is increased, the stability margin is decreased in this figure. After 27.5 kA of the operating current, the stability margin of the old design is higher than that of the new design. This means the area of the superconductor and the copper plays the main role in the stability beyond this limit, while the helium area is the main factor for the stability below this point. Notice that the

Table 4 Definitions of key allowables

Parameter	Definition	Allowable
$E_{headroom}$	Local energy/cable volume needed to raise the local helium from inlet temperature to the current-sharing temperature of the superconductor	>600 mJ/cc
E_{margin}	Local energy/cable volume needed to raise the local helium temperature to current-sharing temperature according to a transient analysis of the local heat deposition and removal during a scenario	>300 mJ/cc

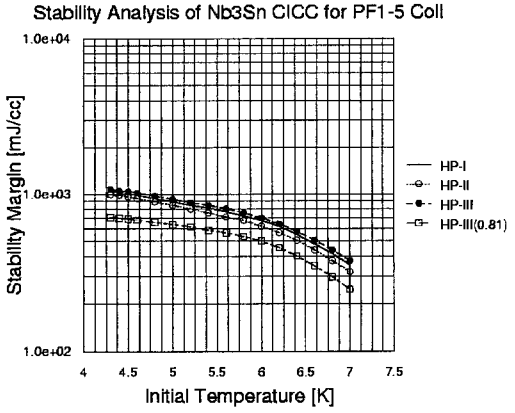

Fig. 7 Initial temperature vs. stability margin

helium area was increased and the area of superconductor and copper was decreased at the new design. Since the maximum operating current for real case is 26.5 kA, HP-III for new design has more advantages compared with other strands.

Figure 7 represents the effect of initial helium temperature on stability margin. The cryogenic conditions and geometry are the same as in the previous calculation in Fig. 6, and the operating current is fixed as 26.5 kA. At initial temperature, 5K, the stability margin of HP-III in the new design is 928 mJ/cc, and its value is still three times larger than design criteria. Since the low helium temperature has more cooling capacity, when the initial temperature is increased, the stability margin is decreased. Also, four curves show a same shape with respect to the variations of the initial temperature and their magnitudes

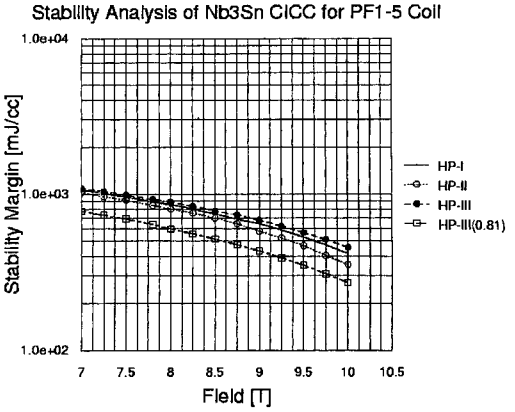

Fig. 8 Field vs. stability margin

show same trend like Fig. 6.

Figure 8 shows the dependence of the stability margin on field strength. The inlet pressure, inlet temperature, operating current, and pulse duration are 5 atm, 5 K, 26.5 kA, and 60 ms, respectively. This figure explains the influence of the critical and current-sharing temperatures, when the field strength is increased. The main sources of instabilities in CICC are AC losses, due to external field changes, or cable motions. Both mechanisms generate heat in the strands. Though the real case works in the transient phenomena, this study is only focused on steady state condition. In order to simulate the transient effect (dB/dt), the field strength between 10 and 8 T, which are larger than 7.8 T of the normal operating field, are used for the parametric study. Their stability margins of HP-III, II, I for the new design and the old design at 7.8 T are 928 mJ/cc, 848 mJ/cc, 894 mJ/cc, and 640 mJ/cc, respectively. The stability margin is improved about 1.5 times at 7.8 T, two times at 10 T by the design change. The stability margin is decreased smoothly as the field strength is increased. The stability curve is quite smooth and limiting current is not observed.

The effect of pulse duration on stability margin is shown in Fig. 9. Cryogenic parameters and operating conditions are used in Table 3. A change in the heating duration for a given energy input corresponds to a change in the energy deposition power. The stability margin decreases

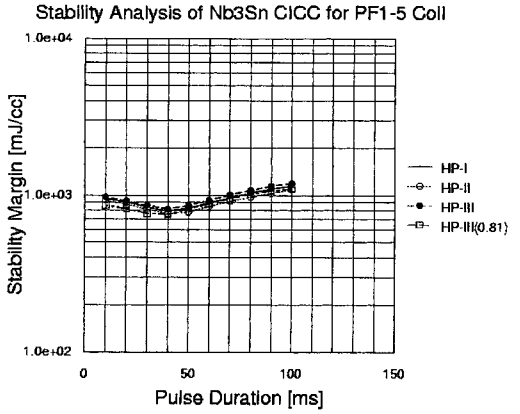

Fig. 9 Pulse duration vs. stability margin

with pulse duration, goes through a minimum at 40 ms, and increases above 50 ms. These physical phenomena exist due to the heat transfer process with transient state in the strands, helium, and jacket and could be explained in terms of the heat diffusion in the thermal boundary layer. Heat transfer to a flow of supercritical helium is fast transient for its relevance to stability. From the experimental (Koizumi, 1993) and theoretical work, the heat transfer coefficient between strand and helium is rapidly changing during the first 10 milliseconds of the strand excursion. Since the recovery or quench after heat input is very fast phenomena, decided in milliseconds after heat input end, thus, the variability of the heat transfer coefficient influences the system behavior. Special care must be considered to the modeling of heat transfer coefficient as a function of time, strand, helium temperature, and helium thermodynamic properties in Eqs. (11) to (18). More detailed formulas for heat transfer coefficient of steady state and transient state are in previous works (Bottura, 1997, Wang, 2000). At 60 ms of reference point, the stability margin for HP-III in the new design is 928 mJ/cc.

5. Conclusions

A zero-dimensional model is effectively used to perform a stability analysis for KSTAR PF coils as a preliminary tool. Parametric studies of ITER HP-I and HP-II, and KSTAR HP-III for Nb3Sn strands were executed as a function of operating current, initial temperature, field, and pulse duration. The strand characteristics of KSTAR HP-III are measured in the Samsung's PPMS and Jc measurement system, and applied for this study. As we expected, the stability margin of HP -III is larger than HP-I, and HP-II. Since the strand diameter was reduced from 0.81 mm to 0. 78 mm due to fabrication process of strand drawing, the stability margin of the new design is larger than the old design at operating conditions. These results are physically reasonable and sufficiently enough for the design criteria. Consequently, the strand type and diameter of CICC for KSTAR PF coils are decided as KSTAR HP-III Nb_3Sn and 0.78 mm. Now, the proposed configuration of CICC has been fabricated underway.

Acknowledgements

This study was supported by the internal research fund of Hannam University.

References

Anderson, P. A., Yin, F. C., and Jones, H, 1983, "The Critical Current Density of Filamentary Nb_3Sn as a Function of Temperature and Magnetic Field," *IEEE Transactions on Magnetics*, Vol. 19, No. 3, pp. 903~906.

Bottura, L., 1997, ZERODEE, A Computer Code for 0-D Stability Analysis, Version 1.1.

Bottura, L., 1991, "Quench Analysis of Superconducting Magnets; A Numerical Study," Ph. D. Dissertation, University of Wales, England.

Bottura, L., 1995, "On the Numerical Studies of Quench in Cable-in-Conduit Conductors," *IEEE Transactions on Applied Superconductivity*, Vol. 5, No. 2, pp. 495~498.

Dresner, L., 1981 "Parametric Study on the Stability Margin of Cable-in-Conduit Superconductors: Theory," *IEEE Transactions on Magnetics*, MAG-17, p. 753.

Gregory, E., 1998, Private Communications, IGC.

KBSI, 1997, KSTAR TSER Presentations, pp.

344~345, Taejon, KOREA.

Koizumi, N., Yoshida, K., Isono, T., Hiue, H., Sasaki, T., Armstrong, J. R., Nishi, M., Shimada, M., Mukai, H., Ono, M., and Wachi, Y., 1993, "Test Results of the DPC-TJ: Stability Performance," *Cryogenics*, Vol. 33, No. 6, pp. 592~596.

Lue, J. W., 1994, "Review of Stability Experiments on Cable-in-Conduit Conductors," *Cryogenics*, Vol. 34, No. 10, pp. 779~786.

Marinucci, C., 1983, "A Numerical Model for the Analysis of Stability and Quench Characteristics of Force-Flow Cooled Superconductors," *Cryogenics*, pp. 579~586.

PPPL (Princeton Plasma Physics Laboratory), 1996, KSTAR Concept Review, Princeton, New Jersey, U. S. A.

SAIT, 1999, KSTAR Magnet System Review, T13&14-22, Taejon, KOREA.

Seeber, B., 1998, *Handbook of Applied Superconductivity*, Volume 1.

Wang, Q., Kim, K., and Yoon, C. S., 2000, "Numerical Model for Thermal Hydraulic Analysis in Cable-in-Conduit-Conductors," *KSME International Journal*, Vol. 14, No. 9, pp. 985~996.

Yoon, C. S., Wang, Q., Kim, K., Baang, S., Kim, S., Park, H., Kim, M., and Choi, H., 2000, "Stability Analysis of Main Coil for Background Magnet in Samsung Superconducting Test Facility," *Proceedings of KIASC conference 2000*, pp. 12~16, Taejon, KOREA.